7. D'Arrigo, R. D., Jacoby, G. C. & Free, R. M. Tree-ring width and maximum latewood density at the North American tree line: parameters of climate change. *Can. J. Forest Res.* **22,** 1290–1296 (1992).
8. Graybill, D. A. & Shiyatov, S. G. in *Climate Since A. D. 1500* (eds Bradley, R. S. & Jones, P. D.) 393–414 (Routledge, London, 1992).
9. Graumlich, L. J. A 1000-year record of temperature and precipitation in the Sierra Nevada. *Quat. Res.* **39,** 249–255 (1993).
10. Cook, E. R., Briffa, K. R. & Jones, P. D. Spatial regression methods in dendroclimatology: a review and comparison of two techniques. *Int. J. Climatol.* **14,** 379–402 (1994).
11. Jones, P. D. & Briffa, K. R. Global surface air temperature variations during the twentieth century: Part 1, spatial, temporal and seasonal details. *Holocene* **2,** 165–179 (1992).
12. Jacoby, G. C. & D'Arrigo, R. D. Reconstructed Northern Hemisphere annual temperature since 1671 based on high-latitude tree-ring data from North America. *Clim. Change* **14,** 39–49 (1989).
13. Jacoby, G. C. & D'Arrigo, R. D. Tree ring width and density evidence of climatic and potential forest change in Alaska. *Glob. Biogeochem. Cycles* **9,** 227–234 (1995).
14. Briffa, K. R., Jones, P. D. & Hulme, M. Summer moisture variability across Europe, 1892–1991: an analysis based on the Palmer Drought Severity Index. *Int. J. Climatol.* **14,** 475–506 (1994).
15. Nicholls, N. *et al.* in *Climate Change 1995* (eds Houghton, J. T. *et al.*) 133–192 (Cambridge Univ. Press, 1996).
16. Groisman, P. Y., Karl, T. R. & Knight, R. W. Observed impact of snow cover on the heat balance and the rise of continental spring temperatures. *Science* **263,** 198–200 (1994).
17. Hogg, P. H. & Hurdle, P. A. The aspen parkland in western Canada: a dry-climate analogue for the future boreal forest? *Wat. Air Soil Pollut.* **82,** 391–400 (1995).
18. Fleming, R. A. & Volney, J. A. Effects of climate change on insect defoliator population processes in Canada's boreal forest: some plausible scenarios. *Wat. Air Soil Pollut.* **82,** 445–454 (1995).
19. DeLuisi, J. J. *et al.* Northern and middle-latitude ozone profile features and trends observed by SBUV and Umkehr, 1979–1990. *J. Geophys. Res.* **99,** 18901–18908 (1994).
20. Sullivan, J. H. in *Stratospheric Ozone Depletion/UV-B Radiation in the Biosphere* (eds Biggs, R. H. & Joyner, M. E. B.) 67–76 (Springer, Berlin, 1994).
21. Tevini, M. in *Stratospheric Ozone Depletion/UV-B Radiation in the Biosphere* (eds Biggs, R. H. & Joyner, M. E. B.) 37–56 (Springer, Berlin, 1994).
22. Bryson, R. A. & Goodman, B. M. Volcanic activity and climatic changes. *Science* **207,** 1041–1044 (1980).
23. Asaturov, M. L. *et al. Volcanoes, Stratospheric Aerosols and Earth's Climate* (Gidrometeoizdat, Leningrad, 1986) [In Russian].
24. Bradley, R. S. & Jones, P. D. in *Climate Since A.D. 1500* (eds Bradley, R. S. & Jones, P. D.) 606–622 (Routledge, London, 1992).
25. Melillo, J. M., Prentice, I. C., Farquhar, G. D., Schulz, E.-D. & Sala, O. E. in *Climate Change 1995* (eds Houghton, J. T. *et al.*) 444–481 (Cambridge Univ. Press, 1996).
26. Hättenschwiler, S., Schweingruber, F. H. & Körner, C. Tree ring responses to elevated CO_2 and increased N deposition in *Picea Abies*. *Plant Cell Environ.* **19,** 1369–1378 (1996).
27. Wigley, T. M. L. Balancing the carbon budget. Implications for projections of future carbon dioxide concentration changes. *Tellus B* **45,** 409–425 (1993).
28. Craig, S. G. & Holmén, K. J. Uncertainties in future CO_2 projections. *Glob. Biogeochem. Cycles* **9,** 139–152 (1995).
29. Ciais, P., Tans, P. P., Trolier, M., White, J. W. C. & Francey, R. J. A large northern hemisphere terrestrial CO_2 sink indicated by the $^{13}C/^{12}C$ ratio of atmospheric CO_2. *Science* **269,** 1098–1102 (1995).
30. Osborn, T. J., Briffa, K. R. & Jones, P. D. Adjusting variance for sample size in tree-ring chronologies and other regional-mean timeseries. *Dendrochronologia* (in the press).

Acknowledgements. We thank P. Nogler, T. Forster, B. Feiertag and E. Schär, WSLFNP, for densitometry and chronology construction, and G. Jacoby and C. Körner for comments on the manuscript. This work was supported by the Swiss Federal Institute of Forest, Snow and Landscape Research, the Swiss National Science Foundation, the European Community Environment and Climate Programme and the UK NERC.

Correspondence and requests for materials should be addressed to K.R.B. (e-mail: k.briffa@uea.ac.uk).

Evidence for partial melt at the core–mantle boundary north of Tonga from the strong scattering of seismic waves

John E. Vidale* & Michael A. H. Hedlin†

* *Department of Earth and Space Sciences, University of California, Los Angeles, Los Angeles, California 90095-1567, USA*
† *Cecil H. and Ida M. Green Institute of Geophysics and Planetary Physics, University of California, San Diego, La Jolla, California 92093-0225, USA*

Scattered waves that precede the seismic phase PKP (which traverses the Earth's core) have been used to identify and locate small-scale heterogeneity in the Earth's mantle[1–6]. A recent study has demonstrated that the global data set of these precursors is consistent with weak heterogeneity (about 1 per cent r.m.s. velocity variation) distributed throughout the mantle[7]. Here we show, however, that anomalously large PKP precursors from earthquakes in northern Tonga require much stronger heterogeneity (10–15 per cent r.m.s. velocity variation) in a layer about 60 km thick near the core–mantle boundary below Tonga. This region of the core–mantle boundary is also marked by low shear-wave velocities in the lower mantle[8] and is near an area of very low compressional-wave velocity in the lowermost tens of kilometres of the mantle[9], which has been interpreted as evidence for the presence of partial melt[10]. The strength of the scattering that we observe provides strong support for the presence of partial melt in this area, and also suggests that vigorous small-scale convection is taking place at the core–mantle boundary.

The nature of the lowermost mantle remains elusive. As the core–mantle boundary (CMB) is the lower bound on mantle convection, it must underlie at least a thermal boundary layer[11]. However, just above the CMB may also be home to chemical heterogeneity[12]. The lowermost mantle shows two kinds of seismic structure. First, layering in P- and S-wave velocities and anisotropy is seen in the few hundred kilometres above the CMB[13]. Second, weak fine-scale heterogeneity is inferred from scattered waves that precede the seismic phase PKP[1–6]. Until recently, the few per cent amplitudes inferred for these two types of structures were small enough that variations in mineralogy and reasonable temperature differences without melt could provide an explanation[7,11,14]. One or more patches of the CMB, which correlate with large-scale slower than average lower mantle, seem to have greater perturbations. Recent work[9,15] suggests P-wave velocity reductions of ~10% in the lowest

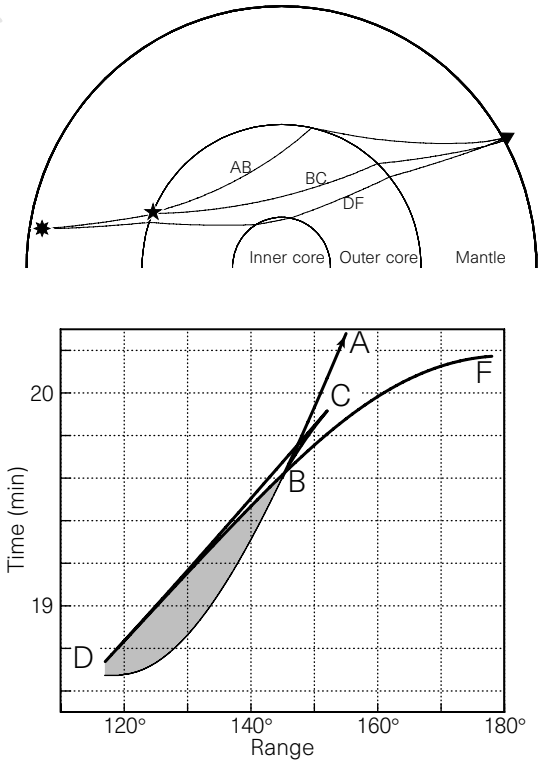

Figure 1 Ray-paths and travel times of PKP phases. A receiver located 140° from an earthquake can detect seismic energy that has passed through the inner core (PKP_{df}) as well as energy deflected from P to the outer core branches PKP_{ab} and PKP_{bc} by a scatterer located at the CMB. Owing to the unusual ray geometries caused by the sharp drop in P-wave velocity at the CMB, this scattered energy can precede PKP_{df}. Although we have depicted near-source scattering at the CMB, scattering at any depth in the mantle at either end of the path can give rise to precursors. The lower panel shows the four branches of PKP from a surface event. In addition to the inner and outer core refracted phases just discussed is PKP_{cd}, the phase that reflects off the inner core. Possible arrival times for the precursors are indicated by the shaded region. In the top panel, the eight-pointed star marks the earthquake, the five-pointed star marks a possible scattering region, and the triangle marks the receiver.

tens of kilometres of the mantle. Such dramatic reductions may indicate the presence of partial melt in the mantle next to the core[10]. Here we present observations of scattered PKP waves requiring large velocity perturbations near the CMB, and note their position beneath low-velocity lower mantle and near a patch exhibiting very slow basal P velocities.

The path that PKP precursors travel through the Earth, by scattering of P waves in the mantle, has been recognized for many years (refs 1–6; Fig. 1). Global surveys of PKP precursors reveal generally weak scattering. For example, near a distance of 136° from earthquakes, within the distance range we analyse, the scattered precursor phases tend to range from 0 to 20% of the amplitude of PKP on short-period recordings[7,16]. The data we present below, however, show much stronger precursors.

In Fig. 2 we show the locations of 22 earthquakes from Tonga and New Hebrides that were recorded on the NORSAR array in Norway. All events were deeper than 100 km and had a moment greater than 10^{26} dyne-cm. The duration of faulting for all events has been measured to range from 4 to 10 s in a study of the rupture properties of deep earthquakes[17]. Three eligible events were discarded; one recording was too noisy, and the other two earthquakes had gradual beginnings that were comparable to the interval between PKP and its precursors.

Anomalous PKP precursors are shown in Fig. 3a and b. The precursors are nearly as large as the PKP waves, and lack long-period energy. The precursors and PKP waves arrive with differing apparent velocities, and the precursors are not as coherent as the PKP waves. The time function of rupture in the earthquake, which may be seen in Fig. 3c, does not explain the complexity of the observed stack. Stacks from the 22 events are shown in Fig. 4. It is clear that the precursor becomes so large beyond 138° that the PKP phase becomes difficult to identify. Precursors as close as 136° have amplitudes comparable to PKP.

PKP precursors in a single seismogram may arise from scattering in the mantle either below the source or the receiver[16]: for example, an event from Tonga recorded at NORSAR (event 7 in ref. 6) showed receiver-side precursors. In our case, the region of the mantle that contributes to source-side scattering for Tonga and New Hebrides has some overlap, while the region contributing to receiver-side scattering is nearly identical. Earthquakes in the New Hebrides subduction zone have smaller scattered PKP precursors than earthquakes from Tonga. The largest precursors clearly have greater slowness than PKP. These observations indicate predominantly source-side scattering for the Tonga earthquakes, as had been previously inferred from similar data[18].

There is a remote possibility that structure in the inner core is removing the high-frequency component of PKP (see Fig. 1 for nomenclature) and misleading us into overestimating the strength of the precursors. If so, the inner-core structure would have to be highly anomalous, as comparable precursors are not observed for other paths.

The anomalous scattering zone seen in the records of the Tonga events is geographically limited. PKP precursors sampling neighbouring areas do not show nearly such large precursor amplitudes. The recordings of the events in New Hebrides show smaller precursors than Tongan events, although still bigger precursors than the global average. French nuclear tests in the Tuamotu archipelago 3,000 km to the east show PKP precursors with normal amplitudes. In addition, the strongest precursors arrive as a distinct pulse in time, whereas scattering from a broader zone would produce a more prolonged precursor wavetrain that would not have a minimum between the precursors and PKP.

A possible complication is that the presence of a zone of strong scattering near the CMB could attenuate the PKP phase as well as amplify the precursors in our seismograms. However, we doubt that PKP is greatly attenuated for the following reasons. First, the amplitudes of the PKP phases from Tonga are similar to those of the PKP arrivals from New Hebrides. Second, attenuation of PKP should vary more with earthquake location than generation of precursors, which is not observed.

We model these arrivals as caused by scattering from a random

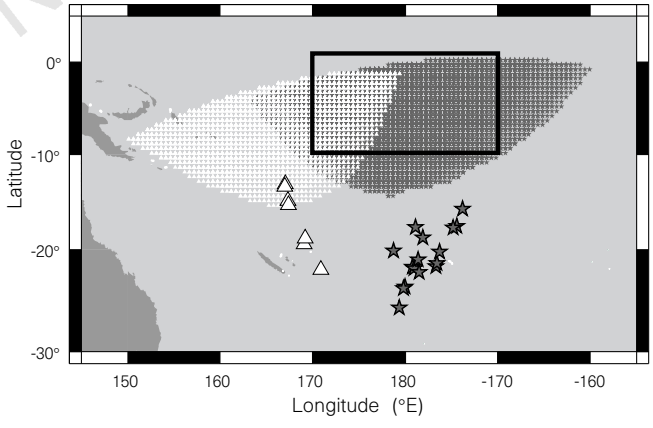

Figure 2 Map of anomalous region of the CMB and the 22 earthquakes used in this study. Dark grey stars indicate Tonga earthquakes, the white triangles represent New Hebrides events. Arcuate regions (shaded to match the event symbols) are the zones on the CMB that contribute to PKP precursors. Parts of Australia are shown to the southwest. The black box is the region inferred to show very strong scattering.

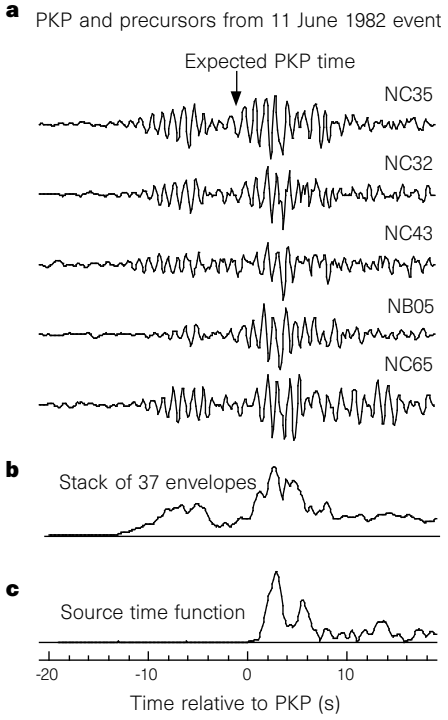

Figure 3 PKP precursor observations. We processed the data as follows: first, the data was filtered in the bandpass from 0.7 to 2.0 Hz to minimize microtremor as well as high-frequency noise; second, we took an envelope of the seismograms, as the data were not suitable for a coherent stack; and third, we stacked the data on the expected slowness of PKP waves. **a**, Five typical filtered seismograms from an event that occurred 136.4° from NORSAR. **b**, Slant stack of the envelopes of the filtered seismograms. **c**, Stack of P waves from California[17] to show earthquake duration.

medium using Chernov's theory[19] adapted to elastic media[4,7]. An alternative possibility is that these precursors to PKP arise from coherent reflections from a dipping planar interface. However, below 0.5 Hz, the precursors in the distance range up to 140° are a factor of ten smaller than PKP. This frequency dependence verifies that the large arrivals we examine are indeed scattered waves.

Our preferred model for the origin of the scattered waves has 13% r.m.s. velocity variations with 10 km scale length in the lowermost 60 km of the mantle across a region at least spanning the box in Fig. 2. Models that extend further up into the mantle or further into the sampled regions do not reproduce the time dependence and thus give poorer data fits. Marginally better fits can be obtained by a model that allows heterogeneous structure only at the CMB. We do not favour this model as it requires still greater velocity variations. The required velocity perturbations scale inversely with the square root of the thickness: for example, the required perturbations scale from 23% for a 20-km-thick patch down to 6% for a patch spanning 250 km. Without lateral variation in the strength of scattering, the observed variations in the precursors that are not simply a function of range cannot be explained. The western edge of the patch limits the predicted amplitudes in the New Hebrides trace. Figure 4 shows the predictions of the preferred model compared to scattering predicted from a model with 1% velocity variations across the entire mantle[7]. The global model predicts far less scattering than is observed. Strong scattering uniformly distributed near the CMB also does not fit the data well.

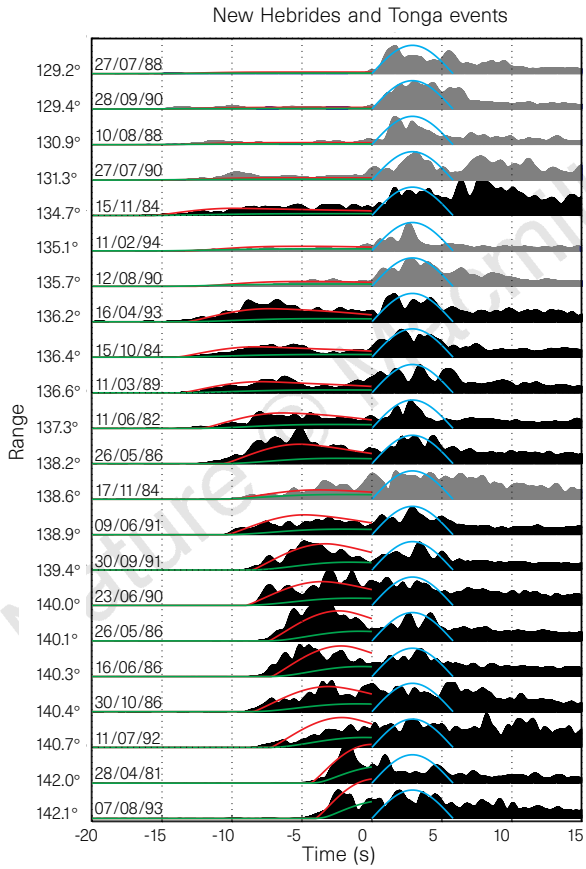

Figure 4 Data and synthetic curves. Stacks of envelopes of bandpassed seismograms for all events are arranged by distance; amplitudes are adjusted downwards by an amount determined by the average energy level of the noise[7], normalized to unity and shifted slightly in time to align PKP. The Tongan records are in black. Dates of events are given as day/month/year. Two sets of calculated envelopes are shown to the left of zero time. The red lines show calculated PKP precursors for 13% r.m.s. velocity variations in the lowermost 60 km of the mantle in the box shown in Fig. 1. The green, lower-amplitude, lines show the calculation for 1% r.m.s. variation across the entire mantle, as determined by a global study[7]. The source-time function is represented by the blue curves to the right of zero time.

Global surveys of PKP precursors have failed to identify regions that scatter as strongly as the region we discuss here. A survey of the data set from a recent publication[7] showed no other paths with PKP precursors larger than 20% of the amplitude of PKP for distances less than 137°. A previous study[16] made the same observation. In contrast, our paths from northern Tonga to NORSAR shows precursors with comparable amplitude to PKP in the range from 136° to 138°, as shown in Fig. 4.

Our initial survey indicates that recordings of PKP precursors that sample low-velocity lower mantle other than the southwest Pacific do not show nearly such large precursor amplitudes. To investigate the CMB under Iceland, we have examined records from NORSAR of French nuclear tests in the Tuamotu archipelago. Their receiver-side scattering zone includes the region below Iceland. These data, mentioned above in reference to their source-side scattering patch, have noticable but minor precursors. Beneath Africa, the most prominent low-velocity feature in the lower mantle[8,20], a spot-check of recordings in Tanzania of Tongan and Mexican earthquakes showed only normal PKP precursors (J. Ritsema, personal communication).

The region that scatters PKP waves lies in the 'equatorial Pacific plume group' (ref. 8) structure which is distinguished by low S-wave velocities in the lowermost several hundred kilometres of the mantle. P-wave tomography of this region[21] also shows lower than average velocities. The low velocities imply hotter than average mantle. In fact, the 'equatorial Pacific plume group' structure that we sample and the 'great African plume' (ref. 8) structure under Africa are probably the two hottest spots at the base of the mantle. However, the S- and P-wave speed anomalies are only 3% and 1%, respectively.

The region about 1,000 km to the southeast of our study area has been inferred to have layering at the base of the mantle with 10–20% reduction in the lowermost tens of kilometres (refs 9, 15), which has been interpreted as partially molten mantle[10], although some argue that it may be difficult to melt the lowermost mantle[22]. The CMB in some other regions, in contrast, appears free of strong scattering[23].

The 13% r.m.s. amplitude of the P-wave velocity variations in our scattering region require the presence of partial melt[10], as other possibilities that could explain weaker velocity heterogeneity at the base of the mantle do not work[12]. In addition, the large lateral gradients in velocity are likely to be accompanied by significant lateral gradients in density. The simplest way to maintain such structure is vigorous convection within the thermal boundary layer at the base of the mantle. □

Received 2 June 1997; accepted 13 January 1998.

1. Haddon, R. A. W. Corrugations on the CMB or transition layers between inner and outer cores? *Eos* **53,** 600 (1972).
2. Cleary, J. R. & Haddon, R. A. W. Seismic wave scattering near the core-mantle boundary: a new interpretation of precursors to PKP. *Nature* **240,** 549–551 (1972).
3. Doornbos, D. J. & Husebye, E. S. Array analysis of PKP phases and their precursors. *Phys. Earth Planet. Inter.* **5,** 387–399 (1972).
4. Haddon, R. A. & Cleary, R. J. Evidence for scattering of seismic PKP waves near the core-mantle boundary. *Phys. Earth Planet. Inter.* **8,** 211–234 (1974).
5. King, D. W., Haddon, R. A. W. & Cleary, J. R. Array analysis of precursors to PKIKP in the distance range 129° to 142°. *Geophys. J. R. Astron. Soc.* **37,** 157–173 (1974).
6. Husebye, E. S., King, D. W. & Haddon, R. A. W. Precursors to PKIKP and seismic wave scattering near core-mantle boundary. *J. Geophys. Res.* **81,** 1870–1882 (1976).
7. Hedlin, M. A. H., Shearer, P. M. & Earle, P. S. Seismic evidence for small-scale heterogeneity throughout the Earth's mantle. *Nature* **387,** 145–150 (1997).
8. Su, W. J., Woodward, R. L. & Dziewonski, A. M. Degree-12 model of shear velocity heterogeneity in the mantle. *J. Geophys. Res.* **99,** 6945–6980 (1994).
9. Garnero, E. J. & Helmberger, D. V. Seismic detection of a thin laterally varying boundary layer at the base of the mantle beneath the central-Pacific. *Geophys. Res. Lett.* **23,** 977–980 (1996).
10. Williams, Q. & Garnero, E. J. Seismic evidence for partial melt at the base of the Earth's mantle. *Science* **273,** 1528–1530 (1996).

11. Jeanloz, R. & Richter, F. M. Convection, composition, and the thermal state of the lower mantle. *J. Geophys. Res.* **84,** 5497–5504 (1979).
12. Manga, M. & Jeanloz, R. Implications of metal-bearing chemical boundary layer in D″ for mantle dynamics. *Geophys. Res. Lett.* **23,** 3091–3094 (1996).
13. Lay, T. Structure of the core-mantle transition zone; a chemical and thermal boundary layer. *Eos* **70,** 49–49 (1989).
14. Loper, D. E. & Lay, T. The core-mantle boundary region. *J. Geophys. Res.* **100,** 6397–6421 (1995).
15. Mori, J. & Helmberger, D. V. Localized boundary layer below the mid-Pacific velocity anomaly identified from a PcP precursor. *J. Geophys. Res.* **100,** 20359–20365 (1995).
16. Bataille, K. & Flatté, S. M. Inhomogeneities near the core-mantle boundary inferred from short-period scattered PKP waves recorded at the global digital seismograph network. *J. Geophys. Res.* **93,** 15057–15064 (1988).
17. Vidale, J.E. & Houston, H. The depth dependence of earthquake duration and implications for rupture mechanisms. *Nature* **365,** 45–47 (1993).
18. Doornbos, D. J. & Vlaar, N. J. Regions of seismic wave scattering in the Earth's mantle and precursors to PKP. *Nature* **243,** 58–61 (1973).
19. Chernov, L. A. *Wave Propagation in a Random Medium* (trans. Silverman, R. A.) (McGraw-Hill, New York, 1960).
20. Grand, S. P. Mantle shear structure beneath the Americas and surrounding oceans. *J. Geophys. Res.* **99,** 11591–11622 (1994).
21. van der Hilst, R., Widiyantoro, S. & Engdahl, E. R. Evidence for deep mantle circulation from global tomography. *Nature* **386,** 578–584 (1997).
22. Zerr, A., Serghiou, G. & Boehler, R. Melting of $CaSiO_3$ perovskite to 430 kbar and first in situ measurements of lower mantle eutectic temperatures. *Geophys. Res. Lett.* **24,** 909–912 (1997).
23. Vidale, J. E. & Benz, H. M. A sharp and flat section of the core-mantle boundary. *Nature* **359,** 627–629 (1992).

Acknowledgements. We thank H.-C. Nataf for a review; Q. Williams, S. Grand, E. Garnero, P. Shearer and D. Helmberger for discussions; J. Fyen and J. Torstveit for supplying the NORSAR data; and J. Ritsema for evaluating the PKP precursors from Tanzanian stations. This work was supported by the US NSF.

Correspondence and requests for materials should be addressed to J.E.V. (e-mail: vidale@ucla.edu).

The breeding structure of a tropical keystone plant resource

John D. Nason*, E. Allen Herre† & J. L. Hamrick‡

* *Department of Biological Sciences, University of Iowa, 312 Chemistry Building, Iowa City, Iowa 52242, USA*
† *Smithsonian Tropical Research Institute, Apartado 2072, Balboa, Ancon, Republic of Panama*
‡ *Departments of Botany and Genetics, University of Georgia, Athens, Georgia 30602, USA*

Despite the recognized importance of maintaining viable populations of keystone plant resources in tropical wildlife parks and forested preserves, the critical question of what constitutes effective breeding units of these species has not been directly addressed. Here we use paternity analysis techniques to reconstruct the genotypes of pollen donor trees and to estimate pollen dispersal distances and breeding population size parameters for Panamanian populations of seven species of monoecious strangler figs (*Ficus*, Moraceae), a particularly widespread and influential group of keystone producers[1–3]. Despite the minute size (1–2 mm) and short lifespan (2–3 d) of the species-specific wasp pollinators (Agaonidae, Chalcidoidea), pollen dispersal was estimated to occur routinely over distances of 5.8–14.2 km between widely spaced host trees. As a result of such extensive pollen movement, breeding units of figs comprise hundreds of intermating individuals distributed over areas of 106–632 km^2, an order of magnitude larger than has been documented for any other plant species. Moreover, these results should be generalizable to the 350 or so monoecious fig species that share this pollination system[4]. The large areal extent of breeding units of these keystone plant resources has important implications for our understanding of both the evolution of tropical biodiversity and its maintenance by applied conservation efforts.

Like a keystone supporting an archway, keystone tropical plant resources fruit all year round and so support a broad spectrum of vertebrate frugivores during times of food scarcity. Figs are considered to be the pre-eminent group of keystone plant resources in southeast Asia and in the Neotropics owing to their heavy fruit production and generally aseasonal patterns of reproduction[1–3]. Given their disproportionately strong influence on species assemblages at many trophic levels, a failure to maintain viable fig populations in forest preserves is expected to result in a cascade of subsequent extinction events[2]. Information guiding the establishment of reserve areas sufficient for the long-term preservation of fig populations is therefore of vital importance to the management of tropical biodiversity, particularly as large areas of continuous tropical forest become increasingly fragmented by human activity.

We have examined spatial patterns of effective fig wasp and pollen dispersal by using paternity analysis techniques to reconstruct precisely the isozyme genotypes of pollen donors fertilizing the fruit of individual fig trees. The research was conducted on populations of seven monoecious fig species (subgenus *Urostigma* sect. *Americana*) and their wasps (genus *Pegoscapus*) occurring in central Panamá. Adults of the fig species studied, *F. citrifolia*, *F. dugandii*, *F. nymphiifolia*, *F. obtusifolia*, *F. perforata*, *F. pertusa* and *F. popenoei*, occur at average population densities of less than ten individuals per square kilometre on Barro Colorado Island (BCI; C. Handley and E. Kalko, unpublished census data)[5,6], a large, 15-km^2 nature preserve located within the study area. Typical of monoecious figs, these species are obligately outcrossing and produce large fruit crops with reproduction synchronous within individual trees but asynchronous between trees[6,7], so that co-flowering individuals are often located substantial distances apart.

The power to reconstruct pollen donor genotypes was facilitated by high levels of assayable genetic variation and access to full-sibling

Table 1 Genetic diversity and probabilities of paternity exclusion

Ficus sp.	Genetic diversity*	Possible isozyme genotypes	Paternity exclusion probability: Single offspring	Paternity exclusion probability: Full-sib progeny array†
F. citrifolia	0.258	15,360	0.769	0.997
F. dugandii	0.235	73,728	0.830	>0.999
F. nymphiifolia	0.169	15,360	0.720	0.995
F. obtusifolia	0.231	13,271,040	0.887	>0.999
F. perforata	0.227	331,776	0.912	>0.999
F. pertusa	0.258	31,104	0.869	>0.999
F. popenoei	0.223	20,736	0.821	>0.999

The precision with which pollen donor genotypes was reconstructed was facilitated by highly variable genetic marker loci and access to single foundress, singly sired fruit. Based on observed genetic diversity and allelic variation, thousands of multilocus allozyme genotypes are possible for each species. As a result, the probability of paternity exclusion, a measure of the power with which the genotype of the actual paternal parent can be distinguished from other putative fathers, is very high (>0.995). This probability is greatly enhanced in the fig species studied because full-sib progeny arrays, as opposed to single offspring, can be used to infer the father's multilocus genotype.
* Calculated as average expected heterozygosity over polymorphic and monomorphic loci.
† Calculated as one minus the probability of genotypic identity.

Table 2 Pollen donor diversity and breeding population size

Ficus species	Trees sampled	No. of fruit per tree	Pollen parents: d_{min}	Pollen parents: $\hat{d}$*	Breeding unit size: $\hat{N}_{d_{min}}$	Breeding unit size: $\hat{N}_{\hat{d}}$*
F. citrifolia	2	35.0	13.0	20.5 (2.7)	182.5	287.8 (38.3)
F. dugandii	1	15.0	11.0	18.0 (3.7)	154.4	252.7 (51.9)
F. nymphiifolia	2	28.5	10.0	23.0 (5.5)	140.4	322.9 (77.0)
F. obtusifolia	7	26.2	17.3	54.3 (5.6)	242.7	762.1 (79.0)
F. perforata	2	20.5	6.0	11.0 (2.7)	84.2	154.2 (37.2)
F. pertusa	2	16.0	10.0	16.0 (2.5)	140.9	224.6 (34.3)
F. popenoei	3	14.0	10.7	28.0 (5.3)	147.7	393.1 (74.0)

The number of functionally male, staminate phase trees in the breeding population surrounding a given maternal tree is indicated by the total number of different pollen parent genotypes represented in its fruit crop (d) and was estimated in two ways, from the observed number of distinguishable paternal genotypes in a sample of singly sired fruit (d_{min}, a lower bound), and, more accurately, from the frequency distribution of different paternal genotypes revealed in such a sample ($\hat{d}$, estimated according to ref. 22). Given the reproductive phenologies of the fig populations studied, the observed patterns of paternity indicate that, despite low population densities, breeding units centred about maternal fig trees consist of hundreds of intermating individuals.
* Standard error in parentheses.